SAO-AXAF-DR-93-053
September 1993
NAS8-36123
Type 1 Document

Final Report

AXAF-I Ghost Ray Study - On Orbit Case

Prepared in accordance with DR# 4

Prepared for:
George C. Marshall Space Flight Center
National Aeronautics and Space Administration
Marshall Space Flight

Submitted by:
Smithsonian Astrophysical Observatory
60 Garden Street
Cambridge, MA 02138

SAO-AXAF-DR-93-053
September 1993
NAS8-36123
Type 1 Document

Final Report

AXAF-I Ghost Ray Study - On Orbit Case

Prepared in accordance with DR# 4

Prepared for:
George C. Marshall Space Flight Center
National Aeronautics and Space Administration
Marshall Space Flight

Submitted by:
Smithsonian Astrophysical Observatory
60 Garden Street
Cambridge, MA 02138

Final Report

AXAF-I Ghost Ray Study - On-Orbit Case

T.J. Gaetz
Smithsonian Astrophysical Observatory
60 Garden Street
Cambridge, MA 02138

2 September 1993

AXAF-I Ghost Ray Study - On-Orbit Case - Summary

T. J. Gaetz

The problem of baffles for control of singly reflected (and nonreflected) ghost rays is considered. The theory of baffle design for Wolter Type I grazing incidence optics is reviewed, and a set of sample baffle parameters is obtained subject to the assumptions of nominal mirror figures and perfect manufacture and alignment of baffles. It is found that baffles forward of the optics (in the thermal precollimator) and between the mirror elements (at the CAP) are sufficient to allow the simultaneous ghost image and vignetting requirements to be satisfied for HRMA shells P1H1, P3H3, and P4H4. However, these baffles are not sufficient for the innermost shell P6H6; at best the requirements are slightly violated and there is no margin for tolerances. The addition of a baffle interior to the P6 space at an axial station about one third of the way forward from the aft end of the paraboloid will allow the ghost ray and vignetting requirements to be met. The minimum ghost ray angles and the vignetting angles are sensitive functions of the baffle positions and radii; tolerances of considerably better than 1 mm will be required. The sensitivities are coupled and correlated; further investigations should be undertaken in order to obtain baffle parameters which, combined with likely achievable tolerances, will minimize the risk of the vignetting/ghost ray requirements not being met. The lightweight carbon-epoxy composite used for thermal baffles has insufficient X-ray opacity to be a suitable material for construction of the controlling X-ray baffles; further study is needed to determine an appropriate material and to investigate its thermal and mechanical implications.

I. Introduction

In this paper I consider the problem of specifying baffles which are sufficient to satisfy the simultaneous vignetting and ghost ray requirements as specified in the AXAF-I *Project Requirements Document (PRD) Level II*:

> **3.2.1.5 – Ghost Image Control.** *The aperture design of the mirror assembly shall prevent any nonreflected or singly reflected rays from impinging within a 15 arcminute radius of the on-axis image at the focal plane of a perfectly aligned HRMA. The apertures shall not interfere with doubly reflected rays incident at angles less than 15 arcminutes.*

> **3.2.1.6 – Vignetting.** *The HRMA design aperture shall prevent any vignetting of the x rays in the central 15 arcminute radius area of the on-axis image at the focal plane, except for the effects of the radial supports.*

In the following I briefly review the properties of single reflection rays for individual mirror elements in the absence of the companion mirror of the mirror pair. The rays are analytically projected to the focal plane; this allows the behavior of the limiting rays to be investigated analytically. Using the information gained from the analytic study, sets of baffle parameters are generated which cover a range of limiting vignetting angle and limiting ghost ray angles.

Rays which miss a paraboloid but reflect once from the corresponding hyperboloid will be called *H single-reflection rays*, or, *H ghosts*. Similarly, rays which have a single reflection from a paraboloidal mirror but miss the corresponding hyperboloid will be called *P single-reflection rays*, or, *P ghosts*. Rays which miss both mirror elements of a mirror pair (and are not otherwise blocked) will be called *nonreflecting rays*, or *N ghosts*. The nonreflected rays will receive little direct attention in the following because designs which control the P and H ghost rays will also control the N ghosts.

II. Single Reflection Rays

In order to understand the behavior of single reflection ghost rays in Wolter Type I systems, it is useful to consider the behavior of reflections off of a single optic. I work in a coordinate system in which the optical axis lies along the Z axis with the focal point at a larger value of Z than the mirror pair; X and Y complete a right-handed coordinate system. The coordinate origin lies at the intersection of the nominal CAP midplane with the optical axis. The location of a mirror element is specified in terms of the axial station of the mirror midplane, the plane intersecting the mirror halfway along its length.

The mirror surface shape can be specified in the form

$$r = \left(r_0^2 + 2K(z - Z_{\rm m}) - P(z - Z_{\rm m})^2\right)^{1/2} \tag{1}$$

where z is an axial coordinate measured relative to $Z_{\rm m}$, the mirror midplane; if the mirror length is L, the points corresponding to the forward and aft edges of the clear aperture are given by $-L/2$ and $L/2$, respectively. The local axial slope for an untilted mirror element is

$$\tan\alpha(z) = \frac{\partial r}{\partial z} = \frac{K - P(z - Z_{\rm m})}{r} \tag{2}$$

where r is the radius given by equation (1).

Consider a set of rays from an off-axis point source at infinity. The ray direction vector is

$$\hat{\mathbf{v}}_i = [\sin\theta\cos\psi, \sin\theta\sin\psi, \cos\theta]\,. \tag{3}$$

The angle θ is the off-axis angle for the source. The variable ψ is an azimuthal coordinate about the optical axis; it is zero in the direction of the $+x$ axis and increases towards the $+y$ axis.

The direction vector for a reflected ray is given by

$$\hat{\mathbf{v}}_r = \hat{\mathbf{v}}_i - 2(\hat{\mathbf{n}}\cdot\hat{\mathbf{v}}_i)\hat{\mathbf{n}}, \tag{4}$$

where $\hat{n}$ is the local surface normal.

In much of the following I use dimensionless coordinates ρ and ζ which are the radius and axial station scaled by the focal length:

$$\rho = r/F, \quad \zeta = z/F. \tag{5}$$

The problem of determining the focal plane intercepts of singly-reflected rays can be simplified by considering a narrow ring at a fixed axial station ζ along the mirror element; the radius of the ring is ρ and the position of a point on the ring is

$$\mathbf{w} = [\rho \cos\phi, \rho \sin\phi, \zeta], \tag{6}$$

ϕ is the azimuth angle about the optical axis; ϕ is zero in the direction of the $+x$ axis and increases towards the $+y$ axis. The local surface normal at the point is

$$\hat{\mathbf{n}} = [\cos\alpha \cos\phi, \cos\alpha \sin\phi, -\sin\alpha], \tag{7}$$

where α is the local axial slope angle defined in Eq. (2).

The reflection condition can be applied for each ray on the ring, and the ray analytically projected to a plane perpendicular to the axis and at distance F. In the present study, F is taken to be the focal length of the mirror pair so that the plane intersects the axis at the position of the best on-axis focus; in dimensionless coordinates, this plane is given by $\zeta = \zeta_{fp} = 1$. The focal surface is actually curved, so the image will not remain in focus as it moves off axis along the plane.

The reflected ray is projected from its surface intercept, $\mathbf{w}$, to the focal plane using

$$\mathbf{w}_{fp} = \mathbf{w} + (1 - \zeta)\frac{\hat{\mathbf{v}}_r}{|\hat{\mathbf{v}}_r|}. \tag{8}$$

The resulting focal plane intersection is

$$\mathbf{w}_{fp} = [\mathcal{R}\cos\phi + \eta\cos\psi, \mathcal{R}\sin\phi + \eta\sin\psi, 1], \tag{9}$$

where

$$\mathcal{R} = \rho + h\left(\frac{1-\zeta}{1-h}\right)\cot\alpha, \tag{10}$$

$$\eta = \left(\frac{1-\zeta}{1-h}\right)\tan\theta, \tag{11}$$

and

$$h = 2\sin\alpha(\sin\alpha - \cos\alpha\tan\theta\sin\phi);$$

h is related to the dot product of the local normal with the incident ray direction vector:

$$\hat{\mathbf{n}}\cdot\hat{\mathbf{v}}_\mathbf{i} = -\frac{h\cos\theta}{2\sin\alpha} \tag{12}$$

Without loss of generality, we can consider point sources at varying values of off-axis angle θ for a fixed value of ψ; the corresponding results for other values of ψ can be obtained by a rotation about the optical axis. For concreteness, I consider off-axis sources confined to the $y-z$ plane so that $\psi = \pi/2$ and $\sin\psi = 1$, $\cos\psi = 0$. Note that for a perfectly aligned system with perfect optics, symmetry implies that the plane containing the optical axis and the off-axis source will also contain the limiting ghost rays and limiting vignetting angles. For fixed values of $\mathcal{R}$, η, and ψ, but allowing ϕ to vary, equation (9) describes a member of a family of limaçons. In actuality, $\mathcal{R}$ and η depend on ϕ through their dependence on h, but in the limit of small α (appropriate for grazing incidence optics) and small θ, the effect of this ϕ dependence is small and the figure is very close to being a limaçon.

Individual mirror elements do not focus rays at the same location as a mirror pair: the paraboloidal mirror elements focus rays behind the mirror pair focal plane, while the hyperboloidal mirror elements focus rays ahead of the pair focal plane (see Fig. 1).

Consider a paraboloidal mirror element by itself (*i. e.*, in the absense of its companion hyperboloid); rays from an on-axis point source at infinity will produce an out-of-focus ring at the (mirror pair) focal plane. In this case, the focus of the optic is behind the system focus so that the $+y$ portion of the out of focus ring is produced by the $+y$ portion of the optic. A hyperboloidal mirror element by itself also produces an out of focus ring; however, because the hyperboloid focuses the rays ahead of the focal plane, the image is inverted and the $-y$ portion of the image is produced by the $+y$ portion of the optic. In both cases, the ring will be delimited by the rays reflecting from the forward and aft edges of the element; see Figure 2.

As the source is moved off axis in the $-y$ direction, the circular images distort, first flattening on the $+y$ side, then forming a cusp to make a cardioid, and finally forming a limaçon. The figures have the same orientation for both mirror elements, and very

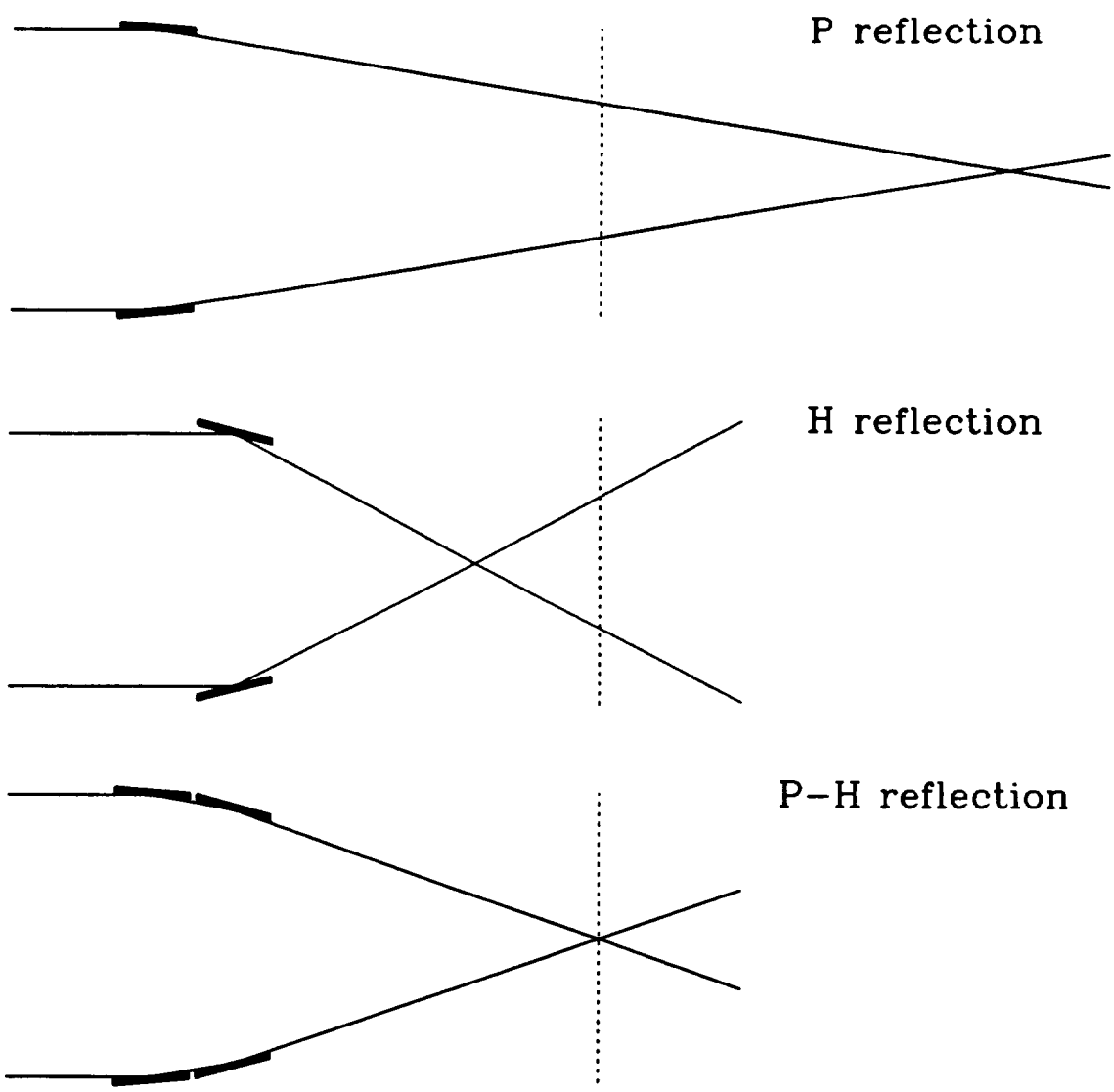

Figure 1 - Schematic diagram of rays reflected from a single P or H mirror element compared to the P and H combination of the Wolter type I design. The dashed line indicates the focal plane for the mirror pair.

nearly the same size (see figure 2). Two extreme points of the curve are the rays in the plane containing the source and the optical axis; these rays satisfy $\cos\phi = 0$,

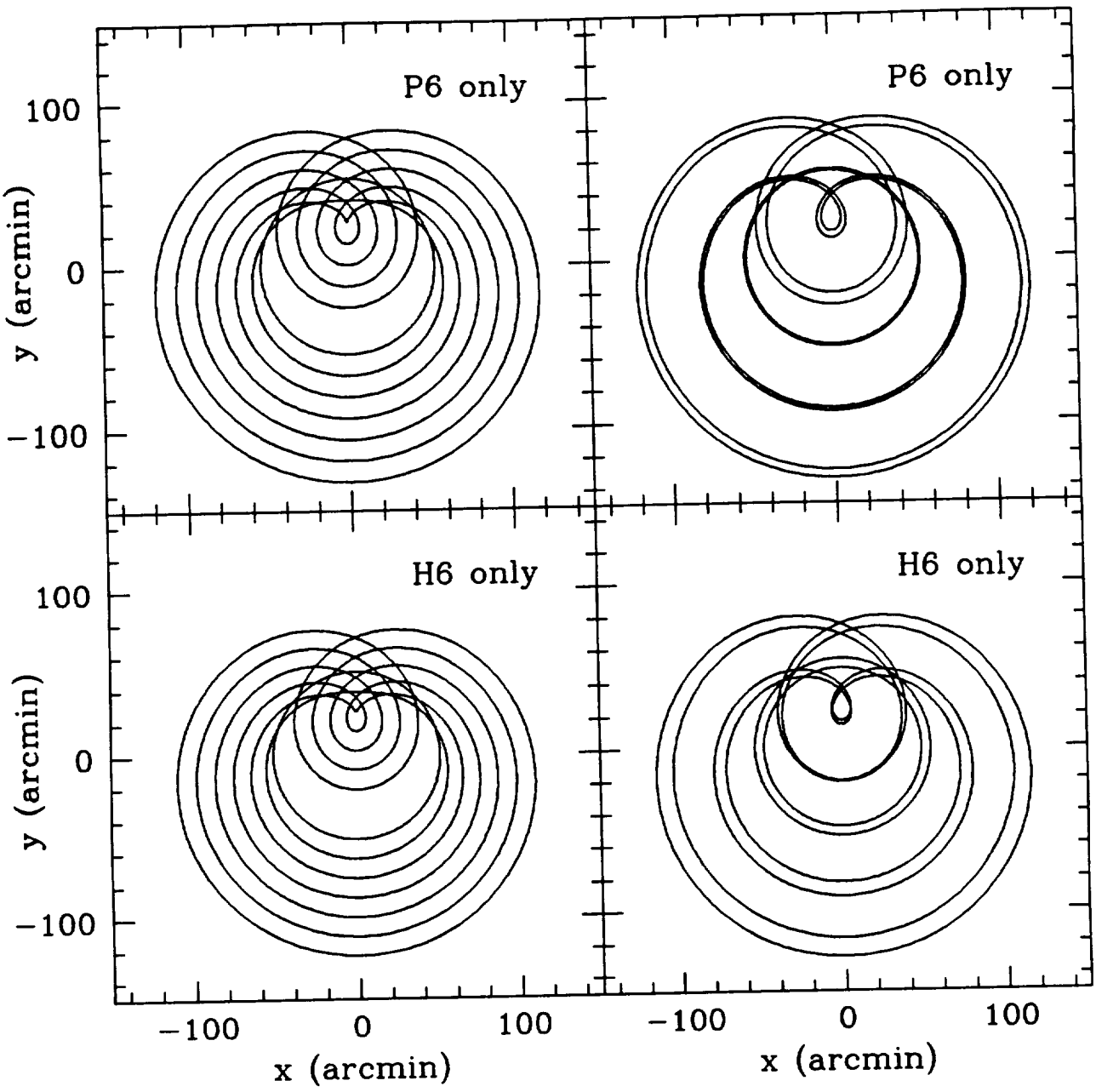

Figure 2 - The left panels shows the images of rays from a point source at infinity and intercepting a mirror element at its midplane; curves are shown for source off-axis angles of 0, 12.5, 25, 37.5, 50, 62.5, and 75 arcmin. The right panels show the images of rays reflecting from the forward and aft edges of an individual mirror element; curves are shown for off-axis angles of 0, 37.5, and 75 arcmin. In each case only a single mirror element of the mirror pair is considered; the companion mirror element is absent.

$\sin\phi = \pm 1$. This condition can be substituted in in equation (9), yielding

$$\rho_{fp} = \rho + (1-\zeta)\tan(2\alpha - \theta) \tag{13a}$$

for the $\sin\phi = +1$ case (*i. e.*, the image of the top $(+y)$ point of the ring), and

$$\rho_{fp} = -\rho - (1-\zeta)\tan(2\alpha + \theta) \tag{13b}$$

for the $\sin\phi = -1$ case (the image of the bottom $(-y)$ point of the ring); ρ_{fp} is the intercept of the ray with the focal plane (in units of the focal length).

The values of $\tan^{-1}(\rho_{fp})$ for the AXAF-I mirror elements are plotted in Fig. 3 . This figure indicates the range of source off-axis angles which potentially contribute to ghost rays in the region about the optical axis; the horizontal dotted lines at ± 15 arcmin indicate the limits of the AXAF-I PRD requirement. The potential contributors to single-reflection P or H ghosts within the central 15 arcmin are listed in Table 1.

Table 1
Potential Point Source Contributors
to Ghosts Within 15 Arcminutes

Mirror Element	Off-Axis Angular Range
P1 or H1	~79 – 120 arcmin
P3 or H3	~61 – 98 arcmin
P4 or H4	~53 – 88 arcmin
P6 or H6	~35 – 70 arcmin

Once the source has moved off axis far enough to form a limaçon, the intersection of the loops forming the limaçon can be found from the condition $\mathcal{R} = 0$:

$$\rho_{fp} = \left(\frac{1-\zeta}{1-h}\right)\tan\theta; \tag{14}$$

for the parameters of interest ($h \ll 1$, $\zeta \ll 1$) this reduces to $\rho_{fp} \simeq \tan\theta$, *i. e.*, the crossing point for the limaçon will lie very close to the focused image of the off-axis source.

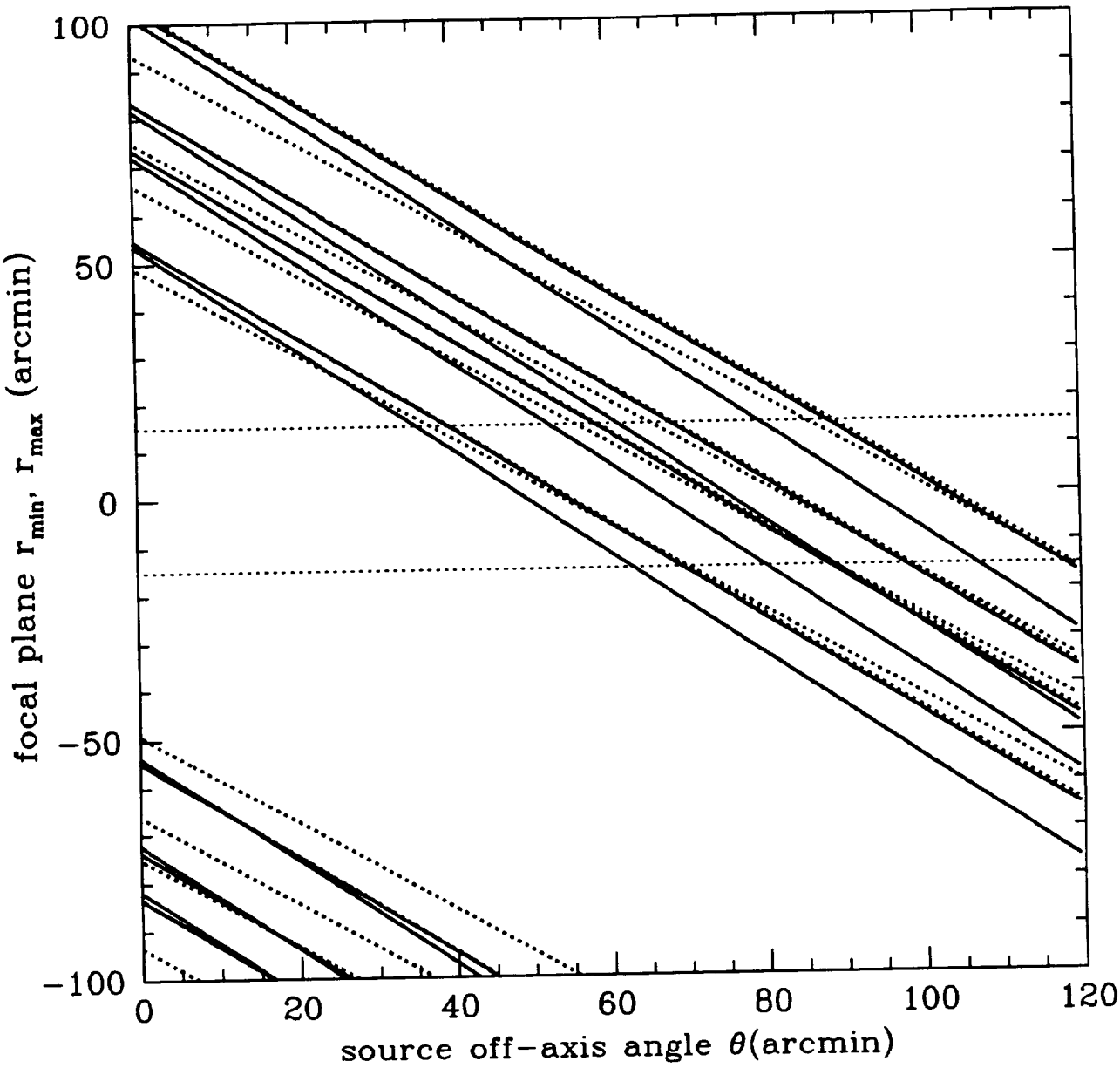

Figure 3 - Critical angles as a function of source off-axis angle (see eqs. (13a) and (13b)). Heavy solid lines: eq. (13a) evaluated for the forward and aft edges of the AXAF-I paraboloids. Heavy dotted lines: eq. (13b) evaluated for the forward and aft edges of the AXAF-I hyperboloids. Horizontal dotted lines: AXAF-I ± 15 arcmin ghost image requirement. The zero crossing increases progressively from shell 6 (P6 or H6) to shell 1 (P1 or H1).

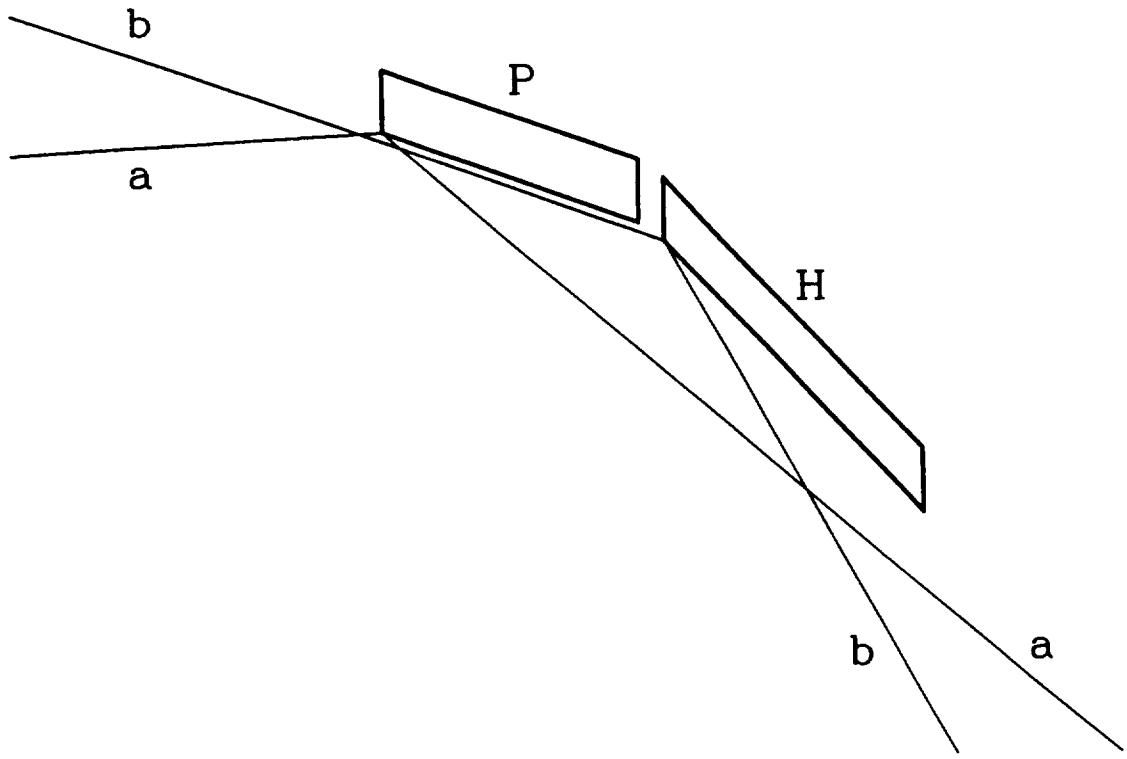

Figure 4 - Schematic diagram of single reflection ghosts. Ray a strikes the parabola with too steep a positive slope and the reflected ray misses the aft end of the hyperbola becoming a "P ghost". Ray b is an example of an "H ghost".

Now consider the mirror pairs assembled into a Wolter Type I mirror pair, assuming perfect mirror surface figures and alignment. Rays from an on-axis source at infinity which hit the paraboloid will also reflect from the hyperboloid and form an image at the pair focal plane. However, any rays from the source which directly hit the hyperboloid will be single reflection rays and unless blocked will become H ghosts (see Fig. 4). Thus, for an on-axis source at infinity, there is no P ghost image and an H ghost (ring) image.

As the source moves off axis in the $-y$ direction, rays striking near the forward $+y$ edge of the paraboloid are reflected too steeply to intercept the hyperboloid; unless blocked, these rays become P ghosts. More of the paraboloid surface contributes to the P ghost image (and more of the limaçon is present) as the source off-axis angle increases.

The loop of the limaçon progresses towards the optical axis and passes through it when the off-axis angle is about twice the surface slope angle for the paraboloid (or two thirds of the surface slope angle for the hyperboloid). Unless additional baffling is provided, the loop will pass through the optical axis and ghost rays will contaminate the central focal plane (see Fig. 3).

III. Ghost Ray Control: Baffle Design

Zombeck, Austin, and Torgerson (1980) consider the utility for ghost ray control of apertures placed in a variety of positions. They consider the following: forward of the optics (in the thermal precollimator), in a plane between the mirror pair, aft of the optics (in the thermal postcollimator), and interior to the paraboloid or hyperboloid spaces (see Fig. 5). They note that the interior baffles are preferable, but that baffling at the forward, centerplane, and aft positions is mechanically more practical. They also note that baffles at the aft location serve to exclude ghost rays *outside* some radius from the optical axis; consequently baffles in the aft location do not help with the problem of satisfying the AXAF-I ghost requirement, and the design of the aft baffles is not further considered here. The Zombeck *et al.* comments are useful but do not provide a quantitative prescription for placement and sizing of baffles. In this section I consider the problem of baffle design for vignetting and ghost ray control; this will be accomplished by determining the limiting ghost rays.

a) Vignetting Conditions

In the case of a perfectly constructed and aligned system, the clear field will be determined by limiting outer baffles forward of the paraboloid: the vignetting of the incoming rays is limited by the baffles at F_i and F_o (see Fig. 5). The baffle F_o together with the forward edge of the paraboloid (P_F) defines a cone with opening (half) angle θ_{Vo} (see Fig. 6). Baffle F_i together with the aft edge of the paraboloid (P_A) defines a cone with opening (half) angle θ_{Vi}; I define θ_{Vo} to be negative and θ_{Vi} to be positive. These angles, θ_{Vo} and θ_{Vi} determine the vignetting limits; there is no aperture-induced vignetting (other than the effect of support spokes) for rays with

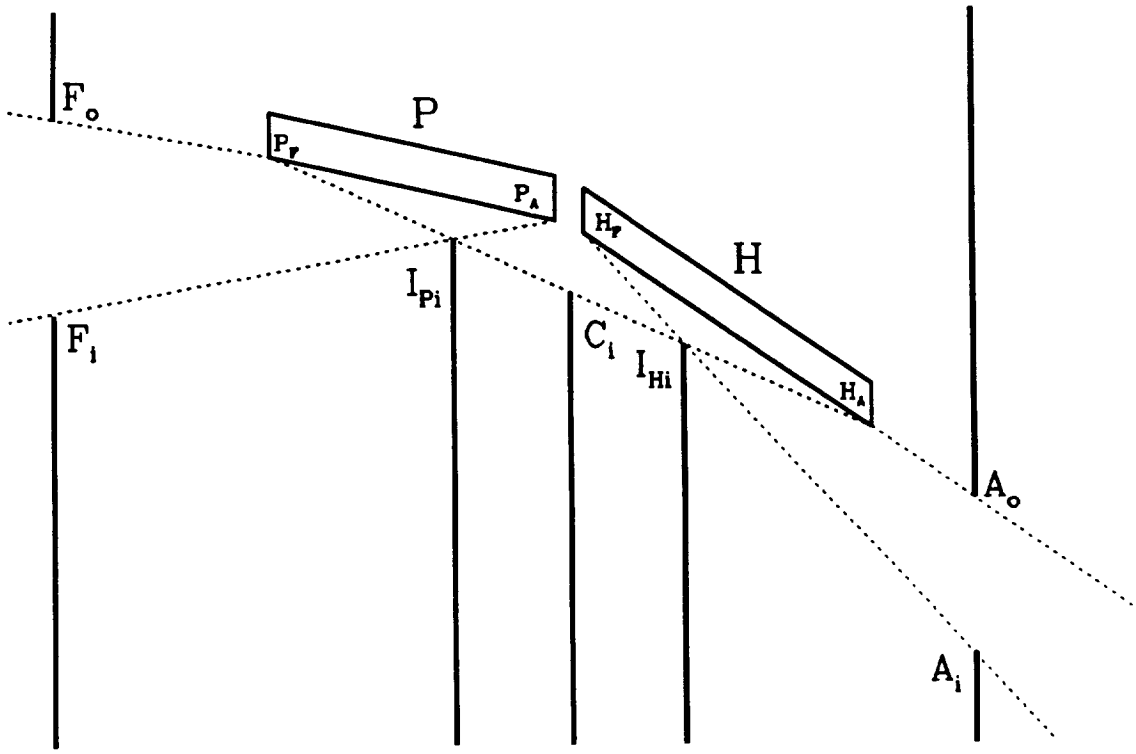

Figure 5 - Schematic diagram of baffles for Wolter type I optics. The dashed lines originating at the forward and aft ends of the optics indicate the vignetting angles. The dashed line connecting the forward edge of the paraboloid (P) to the aft edge of the hyperboloid (H) indicates a limiting "good" ray. Potential baffle locations are forward of the optics (F), between the P and H (C), aft of the optics (A), interior to the paraboloid (I_P), or interior to the hyperboloid (I_H).

angle within $\min(|\theta_{Vo}|, |\theta_{Vi}|)$ of the optical axis. Note that it is possible to use baffle I_{Pi} as a limiting baffle for vignetting but this is undesirable in practice because of the greatly increased sensitivity of the vignetting angle.

The vignetting angles θ_{Vi} and θ_{Vo} are given by

$$\theta_{Vi} = \tan^{-1}\left(\frac{\rho_{Pf} - \rho_{Fo}}{\zeta_{Pf} - \zeta_{Fo}}\right) \tag{15a}$$

and

$$\theta_{Vo} = \tan^{-1}\left(\frac{\rho_{Pa} - \rho_{Fi}}{\zeta_{Pa} - \zeta_{Fi}}\right) \tag{15b}$$

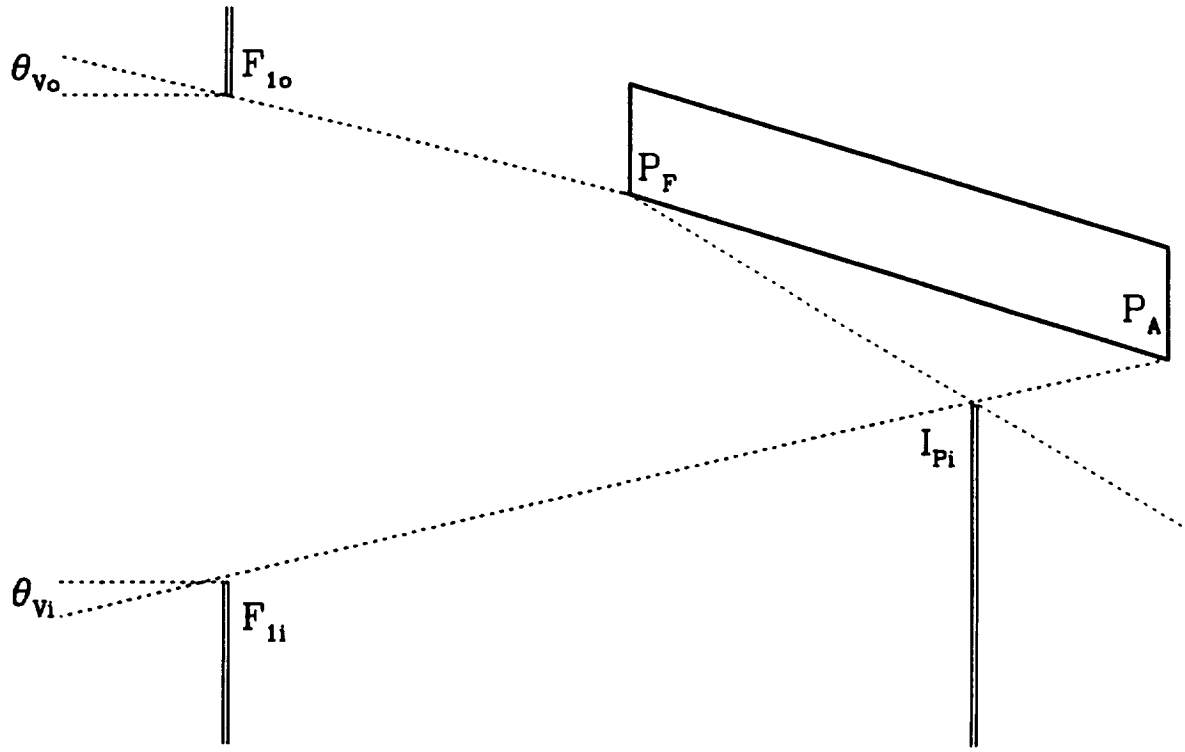

Figure 6 - Schematic diagram of baffles for paraboloid of Wolter type I optics; the limiting angles for vignetting are indicated. The dashed line from P_F to I_{P_i} indicates a limiting good ray extending from the forward end of the paraboloid to the aft end of the hyperboloid.

where the subscripts *Pf* and *Pa* refer to the forward and aft edges, respectively, of the paraboloidal clear aperture, and *Fi* and *Fo* refer to the inner (F_i) and outer (F_o) baffle edges (see Fig. 6).

b) Single Reflection H ghosts

The limiting H ghost ray is determined by baffle F_i and either I_{P_i} or C_i. In the AXAF-I HRMA design, baffling at F_i, F_o, and C_i works for the outer three shells (P1H1, P3H3, and P4H4), but is not adequate for the innermost shell (P6H6). However, it turns out that a baffle at the location I_{P_i} will enable the simultaneous vignetting/ghost ray requirements to be met, at least for ideal conditions. (See Figs. 7 and 8.)

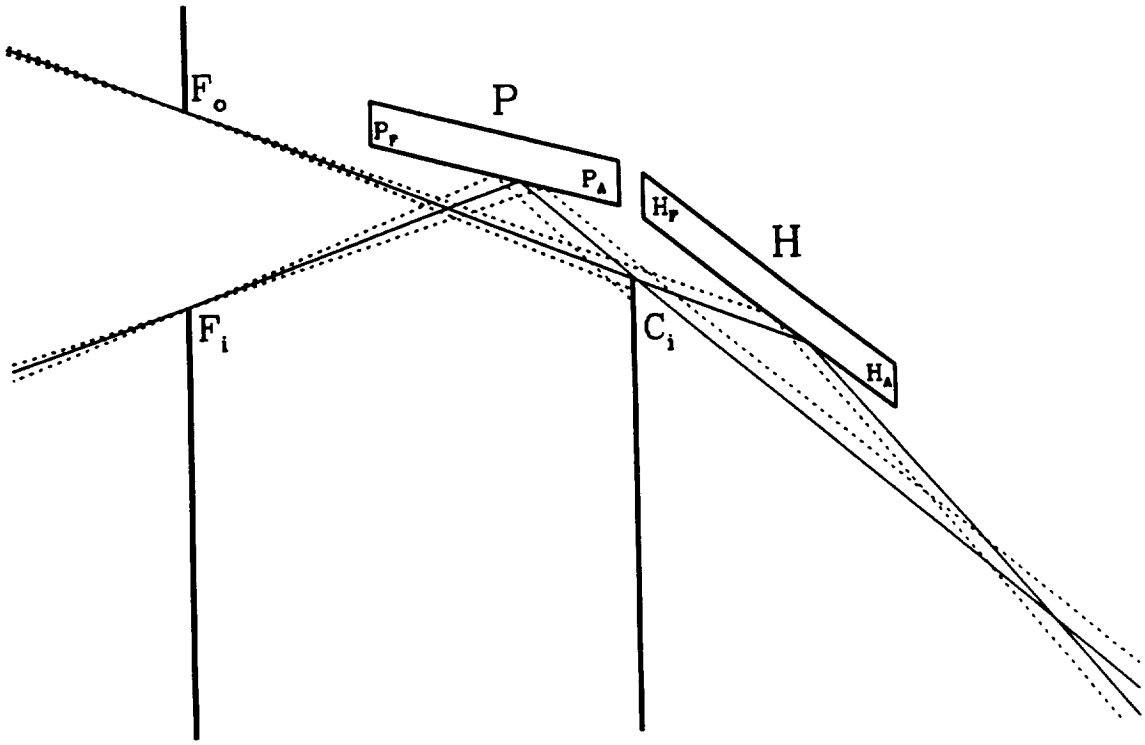

Figure 7 - Control of ghost rays using baffles at F_i, F_o, and C_i. The P ghosts are controlled by the baffles F_i and C_i. The solid curve touching F_i indicates the limiting P ghost ray: steeper rays are blocked by the baffle C_i; shallower rays have a shallower angles after reflection and intercept the focal plane further out than the limiting ray. H ghosts are controlled by the baffles F_o and C_i. The solid curve through F_o indicates a limiting ghost ray: steeper rays are blocked by C_i; shallower rays have a steeper angles after reflection and intercept the focal plane further out than the limiting ray.

Let Z_1 and R_1 refer to the F_i baffle axial station and radius, while Z_2 and R_2 are the corresponding quantities for C_i or I_{Pi} as appropriate. In the $y-z$ plane the incident slope of the limiting H ghost ray is

$$\tan\theta_h = \frac{\rho_2 - \rho_1}{\zeta_2 - \zeta_1}. \tag{16}$$

Steeper incident rays are blocked by the baffles (see fig. 7 and 8). Shallower incident rays are reflected at a steeper angle and intercept the focal plane further out than the limiting ray. I project the limiting ray to its interception (ζ, ρ) with the mirror element; after reflecting from the hyperboloid, the angle is $\phi_h = 2\alpha_h - \theta_h$. The reflected ray is

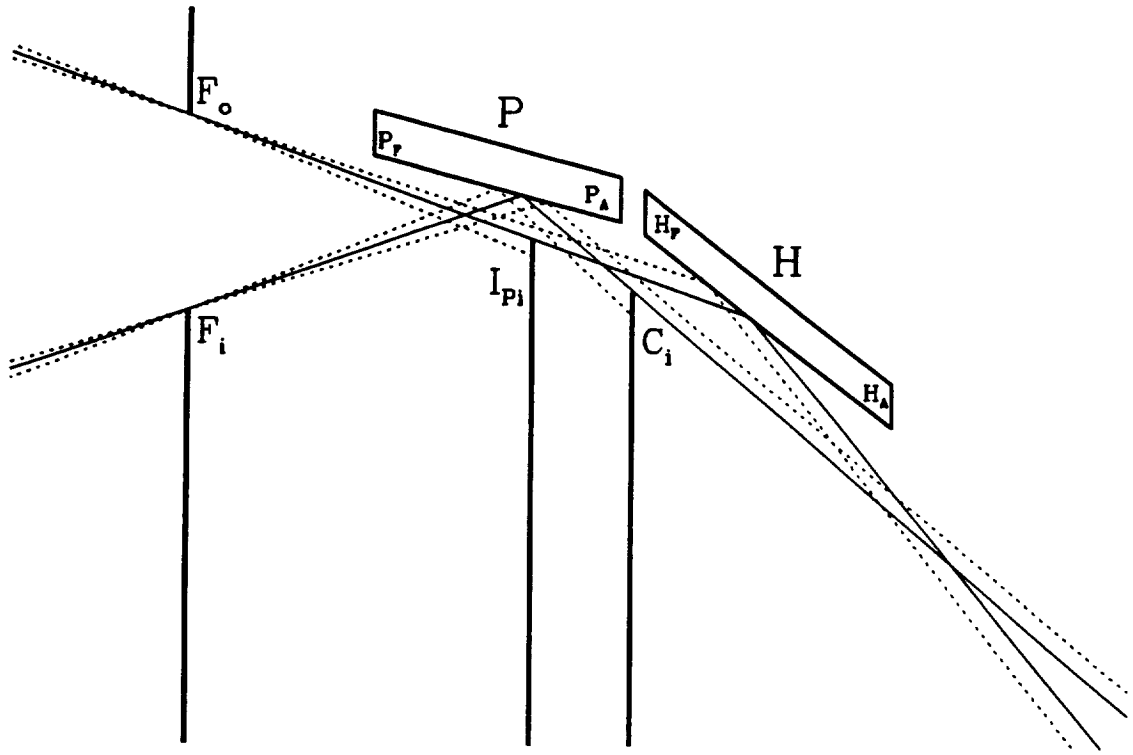

Figure 8 - Control of ghost rays using baffles at F_i, F_o, I_{Pi}, and C_i. The P ghosts are controlled as in figure 7. The H ghosts are controlled by the baffles F_o and I_{Pi}. The solid curve again indicates a limiting ghost ray: steeper rays are blocked by I_{Pi}; shallower rays have a steeper angle after reflection and intercept the focal plane further out than the limiting ray.

projected to ray to the focal plane and the resulting focal plane intercept (converted to an angle) is $\theta_{hg} = \tan^{-1}(\rho + (1-\zeta)\tan\phi_h)$

The addition of a baffle at I_P improves the control of H ghosts by reducing magnitude of the slope of the limiting ray for a given choice of vignetting angle θ_{Vo}; the degree of relief is limited by the need for the baffle to avoid the $F_i - P_A$ vignetting cone and the $P_F - H_A$ cone (see §IIId).

c) Single Reflection P ghosts

The limiting P ghost ray is determined by baffles F_i and C_i. In this case, the intercept

with the mirror surface is between the baffles so simply projecting to the surface will not work. For given baffle parameters I solved for the surface intercept by using a simple "shooting method" and iterating to convergence (fractional difference in radius less than 1×10^{-8}). Again we end up with a limiting ray: steeper incident rays are blocked by one of the the baffles, and shallower incident rays are reflected at a shallower angle than the limiting ray and intercept the focal plane outside the limiting ray. The limiting ray is projected from its mirror surface intercept (ζ, ρ) to the focal plane. The resulting focal plane intercept converted to an angle is $\theta_{pg} = \tan^{-1}(\rho + (1-\zeta)\tan\phi_p)$; θ_p is the angle between the incoming limiting ray and its mirror intercept.

d) Baffle Design Considerations

The choice of radii and axial stations of the controlling baffles F_o and either I_{Pi} or C_i implies a choice of vignetting angle θ_{Vi} and minimum H ghost angle θ_{hg}. Adjusting the radius of the forward outer baffle, R_{Fo}, to improve θ_{hg} will worsen θ_{Vo} and vice versa. Thus, the control of θ_{hg} and θ_{Vo} are anticorrelated. If the other controlling baffle is C_i (as in the case of shells 1, 3, and 4), then the adjustment of R_{Ci} to improve θ_{hg} is limited by the need to avoid the cone $P_F - H_A$: if the baffle protrudes into this cone, the *central* portion of the field at the optical axis will be vignetted. This is highly undesirable, so the baffle C_i will have to be sized to include a margin to avoid this cone. Of course, this margin is at the expense of H ghost control. If a baffle at I_{Pi} is used, as in the case of shell 6, then in addition to a clearance margin for the limiting cone $P_F - H_A$, the baffle should be positioned clear of the $P_A - F_i$ vignetting cone: the I_{Pi} baffle is stationed much closer to the aft edge of the paraboloid than is the F_i baffle; if the I_{Pi} baffle is allowed to become a limiting edge for vignetting, the vignetting sensitivity to baffle radius becomes about four times worse. Consequently, the I_{Pi} baffle should be positioned a bit aft of the ideal station in order to allow a clearance margin for the vignetting cone. The limiting ghost angle, θ_{hg}, is much less sensitive to this margin than to that required to avoid the $P_F - H_A$ cone, so this adjustment of axial station should have relatively little impact on H ghost control.

Similar considerations apply with regard to controlling the P ghosts. If the radius of F_i is adjusted to improve the P ghost control, it is at the expense of the vignetting angle θ_{Vi}. As for the H ghost case, the baffle between the mirrors, C_i, must not interfere with the limiting cone $P_F - H_A$ or the center of the field will be vignetted. Again,

any clearance margin is at the expense of the P ghost angle. A baffle at I_{Hi} would be even better for controlling P ghosts than a baffle at C_i. However, except for the case of the innermost shell, it is mechanically awkward to mount a baffle in this position so it tends to be avoided. It appears that baffling at the C_i position will be adequate for controlling the P6 ghosts. However, the possibility of introducing a baffle at I_{Hi} should be kept in mind in case there are problems in baffling at the location C_i, for example, should the mirror end cut uncertainty introduce too large a margin in the radius of the C_i baffle so that the control of P ghosts is at risk.

The choice of whether to mount the C_i baffle at the forward or aft face of the CAP depends on whether control of P ghosts or H ghosts is more critical (assuming, of course, that the C_i baffle is the limiting baffle for H ghosts). Mounting C_i at the forward face improves the H ghost control; mounting it at the aft face improves the P ghost control.

e) Baffle Material

The controlling X-ray baffles must be opaque to X-rays up to at least 10 keV; note that for some angles the X-rays are controlled by a single baffle. It is evident that the lightweight composite used in constructing the thermal precollimator baffle plates has insufficient X-ray opacity to be a suitable material for the controlling X-ray baffles: preliminary estimates show that a thickness of graphite-epoxy lightweight composite in excess of a centimeter is required in order to attenuate 10 keV X-rays by a factor of 100. The graphite-epoxy composite is thus a poor material for constructing the X-ray controlling baffles.

The controlling baffles must contain sufficient high-Z material to block X-rays, including X-ray energies up to at least 10 keV. For example, a thin layer of high-Z material such as gold or a tungsten alloy might be applied to the critical portions of a lightweight composite thermal baffle plate; alternatively, the baffle plates controlling the X-rays could be made out of a higher-Z material.

Because of the small solid angle subtended by the edges of the controlling baffles as seen at the focal plane, X-ray fluorescence is not expected to be a problem (P. Zhao, private communication).

Control of stray X-rays in general will require that all portions of the observatory within the line of sight of the scientific instruments have sufficient opacity to ensure that stray X-rays do not penetrate and reach the detectors.

Further investigation must be done to determine the appropriate materials and thicknesses of the controlling X-ray baffles and the implications for the thermal and mechanical designs.

IV. Baffle Models for AXAF-I

For the outer shells, the vignetting and ghost requirements can be satisfied with appropriate choices of baffles at F_i, F_o, and C_i. In the case of the innermost shell, P6H6, the simultaneous ghost ray and vignetting requirement cannot be met using only baffles at these locations; however, the addition of a baffle interior to the paraboloid at I_{P_i} will allow the requirements to be met.

Limiting P-ghost and H-ghost angles for P6 and H6 as a function of vignetting angle are plotted in Fig. 9. The baffle positions for a subset of these models (and also for mirror pairs 1, 3, and 4) are listed in Table 2. The forward baffle (F) is assumed to be at -1485.5063 mm from the CAP centerplane, approximately half way between the first two baffle plates in the nominal precollimator design (see Gaetz 1993, Appendix C). The CAP baffle is assumed to be attached to the aft edge of the CAP at +25.4 mm from the CAP centerplane; this slightly improves the control of P ghosts. (However, in the sample calculations for shell 6 *without* an interior P baffle at location I_{P_i}, improving the control of the H ghosting is far more important than controlling the P ghosts so the CAP baffle is instead assumed to be attached to the forward face of the CAP at -25.4 mm from the CAP centerplane. Even with this change, the requirement cannot be met without the additional baffle at I_P.)

Fig. 9 shows the tradeoff of vignetting angle versus limiting ghost ray angle for innermost mirror pair; the H-ghost curves are drawn as solid lines and the P-ghost curve is drawn as dotted a line. The diagonal line from $(0,0)$ to $(40,40)$ indicates the condition of equal vignetting angle and limiting ghost ray angle. The vignetting requirement is plotted as a vertical line at 15 arcmin; acceptable solutions must lie

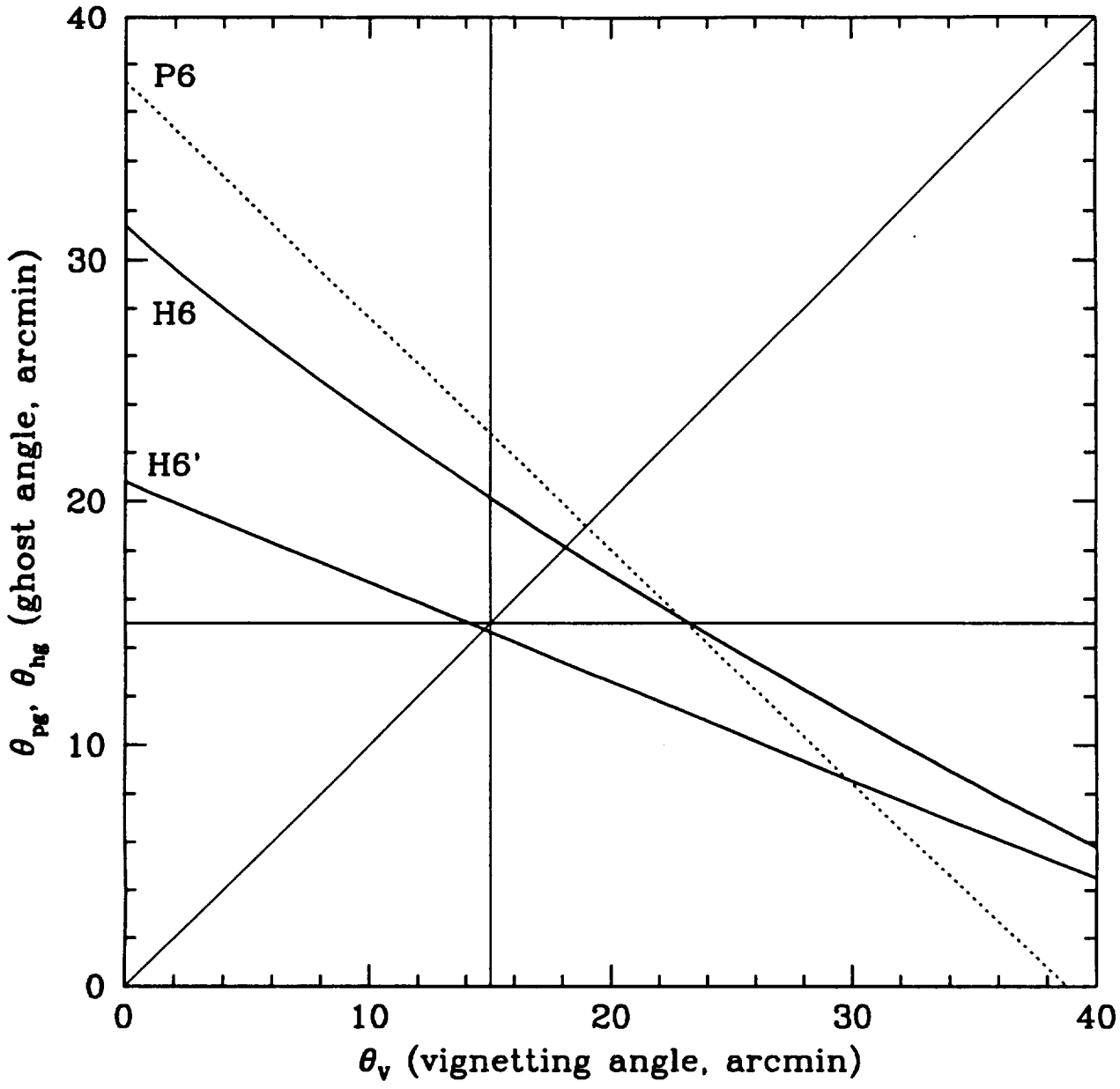

Figure 9 - Limiting P, H ghost angles for P6 and H6 as a function of vignetting angle. Perfect optics and alignment are assumed; all baffles are exactly at their limit locations except for the paraboloid interior baffle for P6, which is 1 mm aft of the optimum position. The z-stations are: F: -1485.50603 mm, C: 25.4 mm (both relative to the CAP centerline = 0.0) The curves are labeled according to the ghost type and mirror element; the curves for P ghosts are dotted and those for H ghosts are solid. The diagonal line at 45° indicates the equal vignetting and ghost angle condition. The H6' curve indicates a case with no interior P baffle. The horizontal and vertical lines indicate the AXAF-I ghost ray and vignetting requirements.

to the right of this line. The ghost ray requirement is plotted as a horizontal line at 15 arcmin; acceptable solutions must lie above this line. It is immediately evident that solutions for the innermost shell which lack the additional baffle at I_P will not work; at best the vignetting/ghost requirements are slightly violated, and there is no room for the error margins which will be needed in constructing and assembling a real HRMA. Adding a baffle at I_P considerably eases the situation: for the P6H6 nominal parameters, designs satisfying the vignetting/ghost requirements are possible ranging from $\theta_V \simeq 15$ arcmin, $\theta_g = \min(|\theta_{pg}|, |\theta_{hg}|) \simeq 20.5$ arcmin to $\theta_V \simeq 24$ arcmin, $\theta_g \simeq 15$ arcmin; the equal vignetting and limiting ghost angle case is $\sim$18.3 arcmin. It is probably desirable to aim for approximately equal vignetting and limiting ghost angles in the design in order to minimize the effects of manufacturing and assembly errors.

Even with the additional baffle, the design and construction of the baffling for P6 and H6 will require great care: preliminary estimates indicate sensitivities of limiting H-ghost angle to baffle radii of about 3 arcminutes/mm, and about 2 arcminutes/mm for the limiting P-ghost angle; the vignetting angle sensitivity is about 2 arcminutes/mm for θ_{V_i} and about 5 arcminutes/mm for θ_{V_o}. Many of the sensitivities are correlated so that the sensitivities add. Because some baffles serve dual rôles in vignetting and ghost ray control, these sensitivities are also coupled. It is already evident that tolerances of considerably better than 1 mm will be needed on the radii and positioning of the X-ray opaque controlling optical baffles. Because of these correlations and coupling, a final baffle design should take into account the sensitivies and the likely achievable tolerances in order to minimize the risk that the final assembled HRMA will violate the simultaneous ghost/vignetting requirements in the final assembled HRMA.

V. Summary and Recommendations

A set of sample baffle designs for the AXAF-I HRMA covering a range of vignetting angle and limiting ghost ray angle has been presented; these designs assume nominal mirror parameters and perfect manufacture and assembly.

It was found that traditional baffling forward of the optics (in the thermal

Table 2

Vignetting and Limiting Ghost Angles (Nominal Case, Perfect Optics, Alignment, and Ideal Baffling)

Shell No.	Case	θ_V (arcmin)	θ_{pg} (arcmin)	θ_{hg} (arcmin)	Z_F (mm)	R_{Fo} (mm)	R_{Fi} (mm)	Z_{Bl} (mm)	R_{Bl} (mm)	Z_C (mm)	R_C (mm)
1	1	10.0000	61.5114	34.5722	-1485.5063	614.44946	596.14814	—	—	25.4	585.96048
	2	15.0000	56.6988	32.5989	-1485.5063	615.32882	594.04966	—	—	25.4	585.96048
	3	20.0000	51.8889	30.6273	-1485.5063	616.20818	591.95115	—	—	25.4	585.96048
	4	25.0000	47.0815	28.6576	-1485.5063	617.08756	589.85260	—	—	25.4	585.96048
	5	30.0000	42.2763	26.6897	-1485.5063	617.96695	587.75402	—	—	25.4	585.96048
	6	35.0000	37.4729	24.7239	-1485.5063	618.84637	585.65537	—	—	25.4	585.96048
	7	40.0000	32.6711	22.7602	-1485.5063	619.72582	583.55667	—	—	25.4	585.96048
	8	45.0000	27.8707	20.7989	-1485.5063	620.60529	581.45790	—	—	25.4	585.96048
	9	50.0000	23.0716	18.8401	-1485.5063	621.48480	579.35904	—	—	25.4	585.96048
3	1	10.0000	47.3853	26.7778	-1485.5063	495.16729	479.26875	—	—	25.4	471.77119
	2	15.0000	42.5767	24.8086	-1485.5063	496.04664	477.17027	—	—	25.4	471.77119
	3	20.0000	37.7714	22.8415	-1485.5063	496.92601	475.07176	—	—	25.4	471.77119
	4	25.0000	32.9690	20.8767	-1485.5063	497.80539	472.97322	—	—	25.4	471.77119
	5	30.0000	28.1690	18.9145	-1485.5063	498.68478	470.87463	—	—	25.4	471.77119
	6	35.0000	23.3712	16.9549	-1485.5063	499.56420	468.77599	—	—	25.4	471.77119
	7	40.0000	18.5752	14.9984	-1485.5063	500.44365	466.67729	—	—	25.4	471.77119
	8	45.0000	13.7807	13.0452	-1485.5063	501.32312	464.57851	—	—	25.4	471.77119
	9	50.0000	8.9876	11.0956	-1485.5063	502.20263	462.47966	—	—	25.4	471.77119
4	1	10.0000	40.6109	23.0753	-1485.5063	437.38804	422.65357	—	—	25.4	416.48587
	2	15.0000	35.8044	21.1080	-1485.5063	438.26739	420.55509	—	—	25.4	416.48587
	3	20.0000	31.0015	19.1432	-1485.5063	439.14676	418.45658	—	—	25.4	416.48587
	4	25.0000	26.2018	17.1810	-1485.5063	440.02613	416.35804	—	—	25.4	416.48587
	5	30.0000	21.4046	15.2219	-1485.5063	440.90553	414.25945	—	—	25.4	416.48587
	6	35.0000	16.6098	13.2660	-1485.5063	441.78495	412.16081	—	—	25.4	416.48587
	7	40.0000	11.8168	11.3139	-1485.5063	442.66440	410.06211	—	—	25.4	416.48587
	8	45.0000	7.0254	9.3659	-1485.5063	443.54387	407.96333	—	—	25.4	416.48587
	9	50.0000	2.2354	7.4225	-1485.5063	444.42338	405.86448	—	—	25.4	416.48587

Table 2 (continued)

Vignetting and Limiting Ghost Angles (Nominal Case, Perfect Optics, Alignment, and Ideal Baffling)

Shell No.	Case	θ_V (arcmin)	θ_{pg} (arcmin)	θ_{hg} (arcmin)	Z_F (mm)	R_{Fo} (mm)	R_{Fi} (mm)	Z_{Bl} (mm)	R_{Bl} (mm)	Z_C (mm)	R_C (mm)
6	1a	10.0000	26.6514	16.6867	-1485.5063	325.57481	313.09330	—	—	-25.4	310.33961
	2a	15.0000	21.6603	14.6457	-1485.5063	326.45416	310.99482	—	—	-25.4	310.33961
	3a	20.0000	16.6735	12.0860	-1485.5063	327.33353	308.89631	—	—	-25.4	310.33961
	4a	25.0000	11.6901	10.5760	-1485.5063	328.21290	306.79777	—	—	-25.4	310.33961
	5a	30.0000	6.7096	8.5486	-1485.5063	329.09230	304.69918	—	—	-25.4	310.33961
	6a	35.0000	1.7315	6.5327	-1485.5063	329.97172	302.60054	—	—	-25.4	310.33961
6	1b	10.0000	27.6041	24.0240	-1485.5063	325.57481	313.09330	-399.55866	316.36054	25.4	309.53938
	2b	15.0000	22.8024	20.6104	-1485.5063	326.45416	310.99482	-373.68515	315.95297	25.4	309.53938
	3b	20.0000	18.0050	17.4350	-1485.5063	327.33353	308.89631	-351.30061	315.60036	25.4	309.53938
	4b	25.0000	13.2113	14.4432	-1485.5063	328.21290	306.79777	-331.74383	315.29229	25.4	309.53938
	5b	30.0000	8.4205	11.5969	-1485.5063	329.09230	304.69918	-314.51074	315.02083	25.4	309.53938
	6b	35.0000	3.6320	8.8690	-1485.5063	329.97172	302.60054	-299.21036	314.77981	25.4	309.53938

precollimator) and between the mirror elements (attached to the CAP) will work for the outermost three shells. The addition of an extra baffle in the interior paraboloid space, about 1/3 of the way from the aft end of the paraboloid, will considerably improve the control of singly-reflected H ghosts and enable the simultaneous vignetting/ghost requirements to be satisfied.

The choice of whether to mount a baffle on the forward or the aft face of the CAP depends on whether control of P ghosts or H ghosts is more critical; mounting C_i at the forward face improves the H ghost control; mounting it at the aft face improves the P ghost control. It is suggested that the CAP baffles be mounted at the *forward* face of the CAP for mirror pairs 1, 3, and 4, and at the *aft* face for mirror pair 6. (In the case of mirror pair 6, the H ghost rays are limited by the interior P baffle rather than the CAP baffle.)

It is desirable to aim for approximately equal ghost ray and limiting ghost angles for each mirror pair in order to minimize the effects of manufacture and assembly errors.

The baffle material must have sufficient opacity to attenuate the X-rays at high energies (10 keV). The lightweight composite material used for the thermal baffles has insufficient X-ray opacity to be suitable for the controlling X-ray baffles; the X-ray baffles will need to include high-Z material (*i. e.*, high atomic weight). Further investigation is needed to determine materials for X-ray baffles and the thermal and mechanical implications.

A preliminary estimate of the sensitivities of vignetting angle and limiting ghost angles to baffle radius indicates that tolerances on radius and positioning of the baffles in the plane perpendicular to the axis will need to be considerably better than 1 mm in order to meet the vignetting/ghost requirements. This will have implications for the design of the thermal precollimator and the inner cylinder; both will need to be structurally sturdy and dimensionally stable enough to maintain the positioning of the controlling X-ray baffles. Further investigation must be done to explore the sensitivities of vignetting and limiting ghost ray angles and their implications for the HRMA design.

References

Advanced X-Ray Astrophysics Facility-Imaging (AXAF-I) Project Requirements Document (PRD) Level II, MSFC-SPEC-1836A, October 16, 1992.

Interim Report, AXAF-I Thermal Precollimator Vignetting Study, SAO-AXAF-DR-93-033, 14 May 1993, T. J. Gaetz.

Interim Engineering Report – High Resolution Mirror Assembly Optical Systems Study, SAO-AXAF-80-003, February 1980, M. V. Zombeck, G. K. Austin, D. T. Torgerson.